Journal of Marine Systems 194 (2019) 25–40

Contents lists available at ScienceDirect

Journal of Marine Systems

journal homepage: www.elsevier.com/locate/jmarsys

A coupled ocean-atmosphere downscaled climate projection for the peninsular Florida region

Vasubandhu Misra[a,b,c,*], Akhilesh Mishra[a,d], Amit Bhardwaj[a,c]

[a] Center for Ocean-Atmospheric Prediction Studies, Florida State University, Tallahassee, FL, USA
[b] Department of Earth, Ocean and Atmospheric Science, Florida State University, Tallahassee, FL, USA
[c] Florida Climate Institute, Florida State University, Tallahassee, FL, USA
[d] Center for Ocean-Atmospheric Science and Technology, Amity University Rajasthan, Jaipur, India

ABSTRACT

A downscaled projection over the Peninsular Florida (PF) region is conducted with a Regional Climate Model (RCM) at 10 km grid spacing that incorporates interactive coupling between the atmosphere and ocean components of the climate system. This is first such application of a coupled ocean-atmosphere model for climate projection over the PF region. The RCM is shown to display reasonable fidelity in simulating the mean current climate and exhibits higher variability both in the ocean and in the atmosphere than the large-scale global model (Community Climate System Model version 4 [CCSM4]), which is used to drive the RCM. There are several features of the regional climate that RCM displays as an improvement over CCSM4: upper ocean thermal stratification, surface eddy kinetic energy of the ocean, volume flux through the Yucatan Channel, and terrestrial rainfall over PF. The projected mean hydroclimatic change over the period 2041–2060 relative to 1986–2005 over PF shows significant difference between RCM and CCSM4, with the RCM becoming significantly drier and CCSM4 moderately wetter. Furthermore, over the ocean surface, especially over the West Florida Shelf (WFS), RCM displays a wetter and a warmer surface climate compared to the CCSM4 simulation.

Our analysis of the model output indicates that improved resolution of ocean bathymetry in the RCM plays a significant role in the response of the projected changes in surface heat flux, clouds, upper ocean circulations and upper ocean stratification, which manifests with some of the largest differences from the CCSM4 projections, especially over the shallower parts of the ocean around PF. This contrast is most apparent between WFS and PF in the RCM simulation, which suggests that a future warm climate would likely produce more rain over WFS at the expense of corresponding reduction over PF, contrary to the absence of any such gradient in the CCSM4 simulation. Furthermore, in the RCM simulation, the warming of the sub-surface ocean in the future climate is owed to the combined influence of excess atmospheric heat flux directed towards the ocean from the atmosphere and the advective heat flux convergence with the relative slowing of the Loop Current in the future climate. The study demonstrates that such RCMs with coupled ocean-atmosphere interactions are necessary to downscale the global climate models to project the surface hydro-climate over regions like PF that have mesoscale features in the ocean, which can influence the terrestrial climate.

1. Introduction

The assessment of regional climate change impacts is of great societal importance as it helps in identifying effective adaptation and mitigation strategies to meet the local risks (Giorgi et al., 2009). The regionalization of the global climate model projections has been traditionally attempted either by dynamic or statistical downscaling methods. Each of these methods has their own benefits and limitations which is discussed in greater detail in Hewitson and Crane (1996) and Wilby and Wigley (1997). In this study, we conduct dynamic downscaling of a global model simulation using a regional coupled ocean-atmosphere model. Many of the earlier dynamic downscaling studies have been conducted with the atmospheric regional models (e.g. Cubasch et al., 1995; Christensen et al., 2007; Mearns et al., 2012) or with oceanic regional models (Somot et al., 2006; Liu et al., 2012, 2015) at a comparatively higher resolution than the driving global models. The intent of these regional dynamic downscaling studies is essentially to direct the computational resources to a subset of the globe (regional domain), thereby allowing for a larger increase in the grid resolution of the regional model to generate locally relevant features of the climate that were likely absent in the coarser global climate model (Denis et al., 2000; Laprise et al., 2008).

A regional coupled ocean-atmosphere model offers further hope in improving the regional simulation by the potential rectification impact of the air-sea interaction of the high-resolution atmosphere and ocean components (Li et al., 2014a, 2014b). This is especially relevant for a region like Florida, that is surrounded by oceans with very robust ocean currents from existence of narrow channels and straits. Liu et al. (2015) and Misra et al. (2016) show that global models display a persistent underestimation of the discharge through the Yucatan Channel and the Florida Straits (see Fig. 1a for their geographical locations). Misra et al. (2017) further indicate that the variability of the flow through these

* Corresponding author at: Department of Earth, Ocean and Atmospheric Science, Florida State University, Tallahassee, FL, USA.
E-mail address: vmisra@fsu.edu (V. Misra).

https://doi.org/10.1016/j.jmarsys.2019.02.010
Received 16 February 2018; Received in revised form 22 February 2019; Accepted 26 February 2019
Available online 28 February 2019
0924-7963/

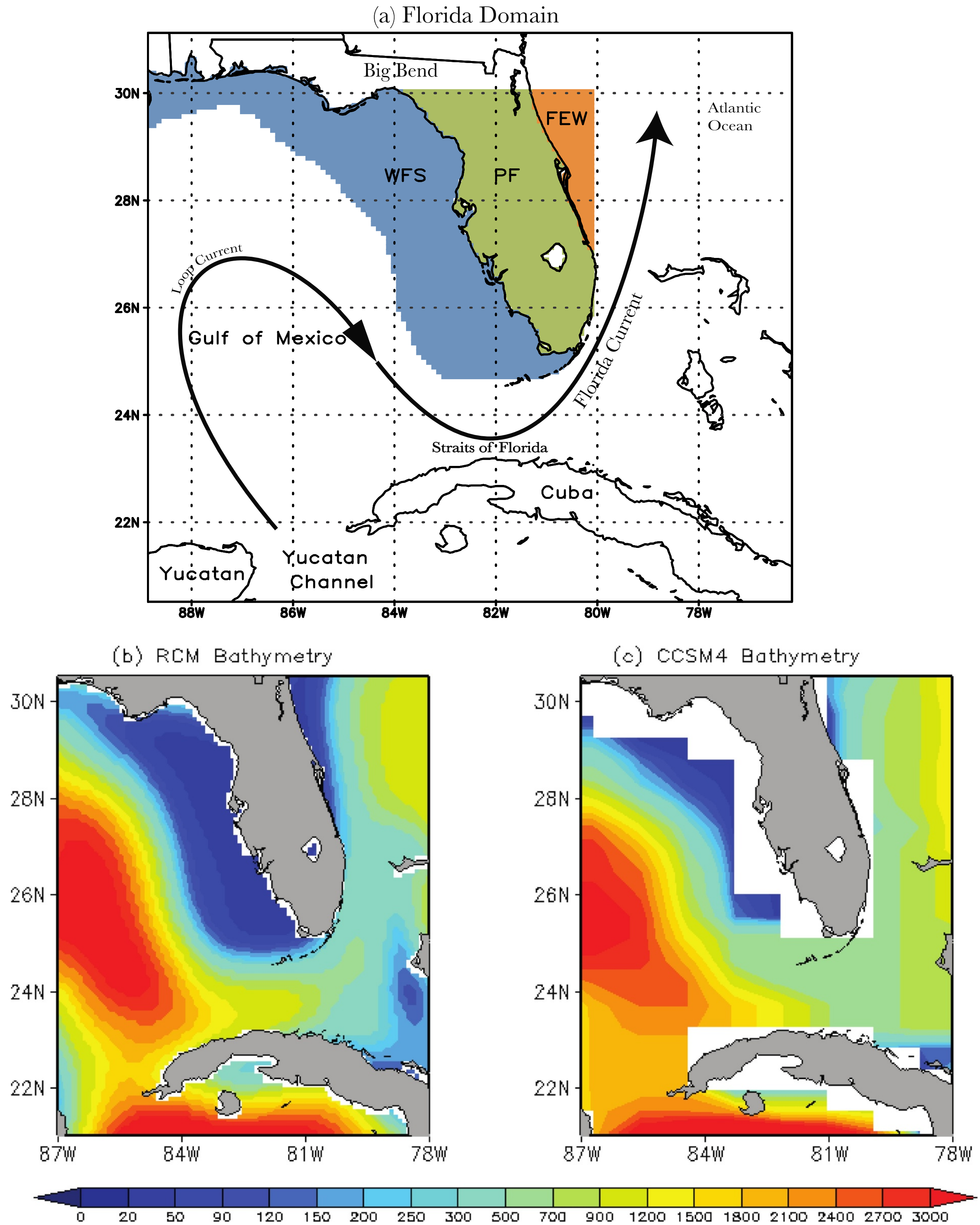

Fig. 1. a) The domain of the model integration with locations of the West Florida Shelf (WFS), the Peninsular Florida (PF) region, and the Florida Eastern Waters (FEW) region. The ocean bathymetry (in meters) at native grids of b) RCM and c) CCSM4.

openings is also underestimated by the global models. Liu et al. (2015) demonstrate that regional ocean models can downscale these global models to produce the ocean currents in this region with higher fidelity. Further, Misra and Mishra (2016) using a regional coupled ocean-atmosphere model demonstrate that SST variations caused by changes in the Florida Current affects the terrestrial hydroclimate over Peninsular Florida (PF). In a related study, Putrasahan et al. (2017) using an eddy permitting global ocean model at 0.1° x 0.1° spatial resolution coupled to a coarser global atmosphere model (0.5° x 0.5°) showed that mesoscale eddies in the Gulf of Mexico (GoM) was important in the upper ocean heat budget. They further indicate that the oceanic mesoscale advection in the GoM sustains SST anomalies that in turn influence the surface heat flux.

Many studies show that a future warm climate could cause significant regional sea level rise in low level areas like Florida on account of the dynamical adjustment of the sea surface to the projected slowdown of the Atlantic Meridional Overturning Circulation (AMOC; Douglas et al., 2001; Vellinga and Wood, 2002; Gregory et al., 2005; Stouffer et al., 2006; Meehl et al., 2007; Yi et al., 2009; Yin and Goddard, 2013). This slowing of the AMOC is significant in the context of this study given that Loop Current is part of its upper branch (see Fig. 1a). In fact, Yin and Goddard (2013) suggest that the mid-Atlantic states are witnessing rapid sea level rise in the recent decades on account of the slowing and northward shift of the Gulf Stream. They further suggest that with the 21st century projected climate forcing, the sea level rise in the mid-Atlantic regions are largely going to be a result of the decline in the density contrast across the Gulf Stream.

The third National Climate Assessment (NCA) report based on analysis of available observations, Coupled Model Intercomparison Projection version 3 (CMIP3) and version 5 (CMIP5), and regional climate projections based on the North American Regional Climate Change Assessment Program (NARCCAP) indicate that there is likelihood of an increase in consecutive number of dry days and an increase in heavy precipitation events over Florida in a future warm climate under the highest emission scenarios (Walsh et al., 2014; Carter et al., 2014). Similarly, over the Caribbean region the model projections indicate a slight decline in the annual rainfall with the boreal summer months displaying the most robust drying signal (Nurse and Sem, 2001; Campbell et al., 2011). Some of these findings have been reiterated in the fourth NCA report (Carter et al., 2018).

In this study, we attempt to downscale a global model simulation for the current and future climate using a Regional Coupled ocean atmosphere Model (RCM) at 10 km grid spacing centered over PF (Fig. 1b). This study is unique to the region that such a tool is being implemented for downscaling climate projection. We analyze the results of this downscaling and compare it with the corresponding global model simulation that is used to drive the RCM at the lateral boundaries. In the following section, we provide a description of the RCM used for the study with a description of the model set up followed by a presentation of the results in Section 3. We then provide a mechanistic explanation for the results of the regional model in Section 4 followed by conclusions in Section 5.

2. Model description and set up

The 20th century historical simulation and the corresponding Representative Concentration Pathway (RCP) 8.5 emission scenario of the Community Climate System Model version 4 (CCSM4) integrations (Gent et al., 2011) was dynamically downscaled for the current (1986–2005) and future mid-century (2041–2060) climate centered over PF to 10 km grid resolution. The RCP8.5 corresponds to the highest greenhouse gas emissions pathway prescribed by the Intergovernmental Panel for Climate Change (Moss et al., 2010). The greenhouse gas emissions and concentrations in this scenario increase significantly over time, leading to a net increase in the radiative forcing of $8.5\mathrm{Wm}^{-2}$ at the end of 2100. The RCP8.5 emission scenario was chosen because the latest global CO_2 emissions continue to track the high end of this emission scenario (Peters et al., 2013).

The dynamic downscaling was conducted with the RCM that follows from Li et al. (2012) with some modifications explained later in this section. The atmospheric component of the RCM is the Regional Spectral Model (RSM; Juang and Kanamitsu, 1994; Kanamaru and Kanamitsu, 2007; Kanamitsu et al., 2010) and the oceanic component is the Regional Ocean Model System (ROMS; Shchepetkin and McWilliams, 2005). A brief outline of the RSM and ROMS is provided in Table 1. It should be noted that some of the changes to the RCM from our earlier studies (Misra et al., 2017) are also included for this study. These changes include changes to the prognostic cloud scheme following Zhao and Carr (1997) that has an additional prognostic equation for cloud water mixing ratio. Furthermore, we have uniformly changed the saturation vapor pressure calculation following Marx (2002) in the RSM to be consistent across all of the subroutines in the RCM. Furthermore, we made changes to calculation of saturation vapor pressure in mixed phase clouds that allowed for a much smoother, linear transition of saturation vapor pressure calculated with respect to water to change to saturation vapor pressure with respect to ice in temperature ranges between 0 °C and − 20 °C before saturation vapor pressure is calculated purely with respect to ice at temperatures below −20 °C. This change in the calculation of the saturation vapor pressure in mixed phase clouds has a profound impact especially on the simulation of high clouds and on the associated cloud radiative feedbacks (Tan et al., 2016; Glazer and Misra, 2018). Additionally, we have changed the coupling interval between the RSM and ROMS in the RCM from one day to every 3 h. The RSM and ROMS in the RCM share identical grids to exchange fluxes and SST without any interpolation at the coupling interval and thus avoiding the use of any couplers. We believe that these flux couplers are a type of an engineering tool that although eases coupling between component models with disparate spatial discretization, can sometimes lead to unwarranted consequences. For example, in the case of CCSM4, the different spatial discretization of the atmospheric and oceanic component leads to the so called "orphaned" grids, which are neither land or ocean points and are often found along the coastlines as depicted by the white spaces in Fig. 1c. However, CCSM4 integrates through without any issues despite such orphaned grids in the domain because of the flux coupler, which manages the passing of the information among the ocean, the land, and the atmospheric components of the model seamlessly, by recomputing either the fluxes or the state variables at the required grid of the interface.

The regional domain for downscaling is indicated in Fig. 1b. The benefit of using the spatial resolution of the RCM over the CCSM4 grid is apparent from comparing Figs. 1b and c, which shows the ocean bathymetry in RCM and CCSM4, respectively. For example, the Florida coastline in CCSM4 (Fig. 1c) is ill defined with a very broad land mass for peninsular Florida relative to the RCM (Fig. 1b). Similarly, the abyss of the GoM, north of the Yucatan Channel and extending further towards Cuba is much deeper in the RCM compared to CCSM4. However, in hindsight the regional domain chosen for RCM in Fig. 1b would have been more ideal if the Loop Current was fully resolved by expanding the domain further westward, say, west of 90°W. In the current configuration, the western boundary of the regional domain would cut through the Loop Current simulation, especially when it is tilted further westward than usual, which then is likely to affect its simulation in the RCM.

The lateral and initial boundary conditions for both RSM and ROMS for the present and the future climate simulations come from the corresponding atmospheric and oceanic components of the CCSM4 simulation. The atmospheric grid resolution of CCSM4 is 1.25° (longitude) x 0.9° (latitude) and for the ocean component in CCSM4 is 1.11° in the zonal direction and in meridional direction varies from 0.27° near the equator to 0.54° at 33°N/S and is held constant at that resolution thereafter in the higher latitudes. The prognostic variables of the atmospheric and oceanic components of CCSM4 are linearly interpolated to the corresponding spatial grids of RSM and ROMS. The lateral boundary conditions for RSM are fed at 6 hour interval while that for ROMS is fed at monthly intervals. We neglect the first year of the RCM integration in consideration of spin-up issues of the upper ocean. Therefore, we use the remaining 20 years of the RCM simulation of the current (1986–2005) and future (2041–2060) climate for analysis with corresponding period from the CCSM4 integration used for comparison.

The evaluation of the simulation of the present climate from CCSM4 and RCM is conducted with the datasets outlined in Table 2. We use overlapping period of the evaluation dataset and the model simulation where possible or resort to using the available climatological period. The objective metrics of Root Mean Square (RMS) errors and bias will be calculated for the 20th century simulations of the RCM and CCSM4 for the masks (PF, West Florida Shelf [WFS], and Florida Eastern Waters

Table 1
A brief outline of the RCM.

	Reference
Atmospheric model (RSM)	
28 vertical terrain following sigma levels with double sine-cosine series with wall boundary conditions as basis functions for horizontal discretization	Juang and Kanamitsu (1994)
Boundary layer	Hong and Pan (1996)
Clouds	Zhao and Carr (1997)
Deep convection	Moorthi and Suarez (1992)
Gravity wave drag	Alpert et al. (1988)
Land Model	Ek et al. (2003)
Longwave radiation	Chou and Lee (1996)
Shallow convection	Tiedtke (1983)
Shortwave radiation	Chou and Suarez (1994)
Ocean model (ROMS)	
30 vertical sigma levels on horizontal staggered Arakawa-C grid	(Haidvogel et al., 2000; Shchepetkin and McWilliams, 2005)
Boundary layer formulation	K-profile (Large et al., 1994)
Mixing scheme	Mellor and Yamada (1982); Umlauf and Burchard (2003)

[FEW]) outlined in Fig. 1a. The evaluation of the model simulations is based on annual mean of the variables except for the volume flux for the Yucatan Channel. This is done for brevity. Furthermore, downscaling a single model does not resolve the uncertainty to provide a robust estimate of the seasonal projected changes. This study is to highlight the importance of resolving air-sea coupling by showing that it causes the divergence of the solution between the global model and dynamically downscaled projections of the climate in the region.

3. Results

3.1. Simulation of the present climate (1986–2005)

3.1.1. Upper ocean climate

The upper ocean extending from surface to approximately a depth of 20 °C isotherm that marks the upper ocean heat content of the tropical-subtropical oceans (Kessler, 1990) is critical for sustaining the mean hydroclimate of PF (Misra and Mishra, 2016). The annual mean climatological SST has comparatively lower values in the northeast GoM, around the big bend region of northern Florida compared to the rest of the GoM (Fig. 2a). In addition, the warm streak of water, east of PF, which is an extension of the Loop Current through the Florida Straits is also visible in the observations (Fig. 2a). The northeast GoM pool of cold water is simulated in the RCM (Fig. 2b) and there is no such cold pool in the CCSM4 (Fig. 2c) simulations. However, the cold bias in the northeast GoM is apparent in the RCM simulation (Fig. 2d). The CCSM4 displays a warm bias along the eastern edge of the WFS and a relatively weaker cold bias all along the Loop Current (Fig. 2e). The RCM however has a cold bias over large parts of the WFS and along the Loop Current (Fig. 2d). But the warm bias over the WFS and the FEW displayed by the CCSM4 (Fig. 2e) is significantly reduced in the RCM simulation (Fig. 2d). The area averaged model bias and RMS errors of

Table 2
Verification datasets for model evaluation.

	Variable	Name of dataset (Acronym used to identify dataset)	Spatial resolution of dataset (zonal x meridional)	Temporal resolution of dataset	Available time period	Source
1	SST	Global High Resolution SST (GHRSST)	5 km × 5 km	Daily	2006–2014	Donlon et al. (2011)
2	Precipitation	TRMM-3B43 (TRMM)	0.25° × 0.25°	Daily	1998–2015	Huffman et al., 1995, 1997; Adler et al., 2000
3	Upper air data	Modern-Era Retrospective Analysis for Research and Applications version 2 (MERRA-2)	0.5° × 0.625°	Daily	1979-present	Suarez and Bacmeister (2015); Reichle and Liu (2014); Wargan and Coy (2016)
4	Sub-surface ocean temperature and currents	Simple Ocean Data Assimilation v2.2.4 (SODA)	0.25° × 0.4°	Monthly	1958–2001	Carton and Giese (2008)
5	Volume flux through Yucatan Channel	RB2010		Climatological monthly mean		Rousset and Beal (2010)

Table 3
Objective metrics of evaluation for 20th century simulations from RCM and CCSM4 for subregions of the domain.

Region	SST				Precipitation			
	RCM		CCSM4		RCM		CCSM4	
	RMS (°C)	Bias (°C)	RMS (°C)	Bias (°C)	RMS (mm/day)	Bias (mm/day)	RMS (mm/day)	Bias (mm/day)
WFS	0.79	−0.3	1.02	0.6	1.05	0.81	0.86	−0.93
PF					0.43	0.1	0.51	−0.46
FEW	0.53	−0.24	0.47	0.4	0.42	0.4	0.09	−0.03

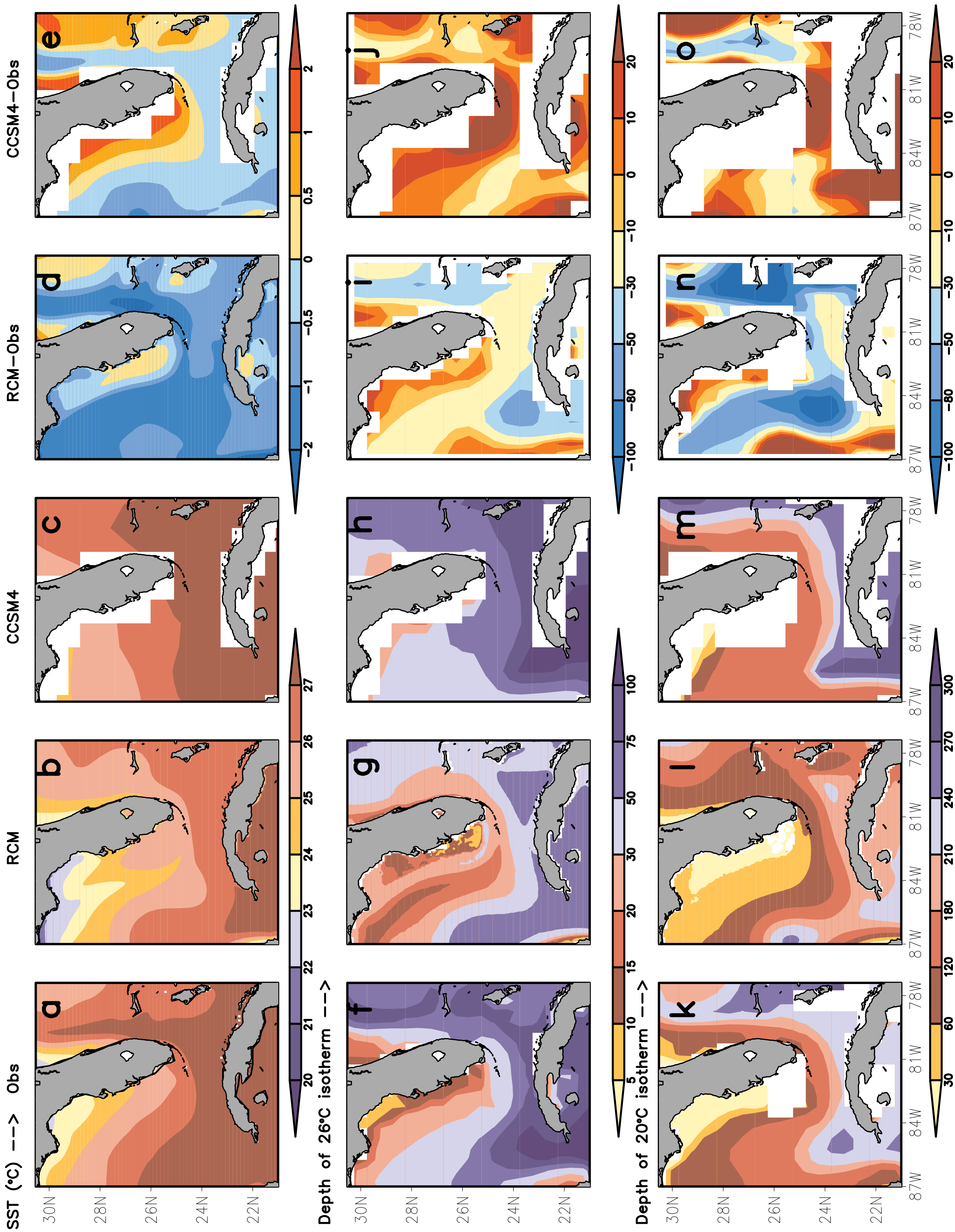
SST (°C) --> Obs
RCM
CCSM4
RCM−Obs
CCSM4−Obs
Depth of 26°C isotherm -->
Depth of 20°C isotherm -->
a
b
c
d
e
f
g
h
i
j
k
l
m
n
o
30N
28N
26N
24N
22N
87W
84W
81W
78W

Fig. 2. The annual mean climatological SST (°C) from a) observations (GHRSST; see Table 2), b) RCM, and c) CCSM4 20th century simulation. The corresponding systematic errors of SST from d) RCM, and e) CCSM4 simulations. Similarly, the annual mean climatological depth of the (f, g, h) 26 °C and (k, l, m) 20 °C isotherm from f, k) observations (SODA; see Table 2), g, l) RCM, and h, m) CCSM4 20th century simulations. The corresponding systematic errors of the depth of the (i, j) 26 °C and (n, o) 20 °C isotherms from i, n) RCM, and j, o) CCSM4 simulations.

SST for RCM and CCSM4 over WFS and FEW is indicated in Table 3, which further confirm our earlier discussion.

The depth of the 26 °C isotherm, which also represents the tropical cyclone heat potential (Leipper and Volgenau, 1972) is shown in Figs. 2f-j. The SODA analysis (Fig. 2f) suggests a shallower depth of 26 °C isotherm along the WFS and over the FEW region relative to that along the Loop Current (over the Florida Straits). This is qualitatively simulated in both model simulations (Fig. 2g and h). The systematic errors however show that the RCM simulation (Fig. 2i) displays a far smaller bias in the depth of the 26 °C isotherm along the Loop Current and along the WFS than the CCSM4 simulation (Fig. 2j), which places the 26 °C isotherm much deeper over these regions. This improvement of RCM over the CCSM4 simulation is further extended to the depth of the 20 °C isotherm, a depth often used as a proxy for ocean heat content (Figs. 2k-o). The systematic errors of the RCM simulation for the depth of the 20 °C isotherm (Fig. 2n) appears from the slight northwestward displacement of the Loop Current relative to SODA reanalysis (Figs. 2k and l). The coarser bathymetry of the CCSM4 reflects the unrealistically wide PF, with the placement of the 20 °C isotherm much deeper than SODA reanalysis in the south and western parts of the regional domain while it is shallower in the eastern part of the regional domain (Fig. 2o).

The surface eddy kinetic energy of the ocean shown in Fig. 3a-c clearly suggests that the RCM simulation has a better representation of this metric than the CCSM4 simulation. It may be mentioned that the ocean currents from the model are interpolated to the SODA grid before the eddy kinetic energy is computed from RCM and CCSM4 in order to make the comparisons fair. Although, estimation of the surface eddy kinetic energy at 0.25° (longitude) x 0.40° (latitude) spatial resolution of the SODA grid is unlikely to yield the true estimate, when the dominant energetic length scale in ocean is about 0.5° (~50 km or submesoscale; Xu and Fu, 2011; Zhong and Bracco, 2013; Sasaki et al., 2014), there is probably some useful information about EKE in SODA

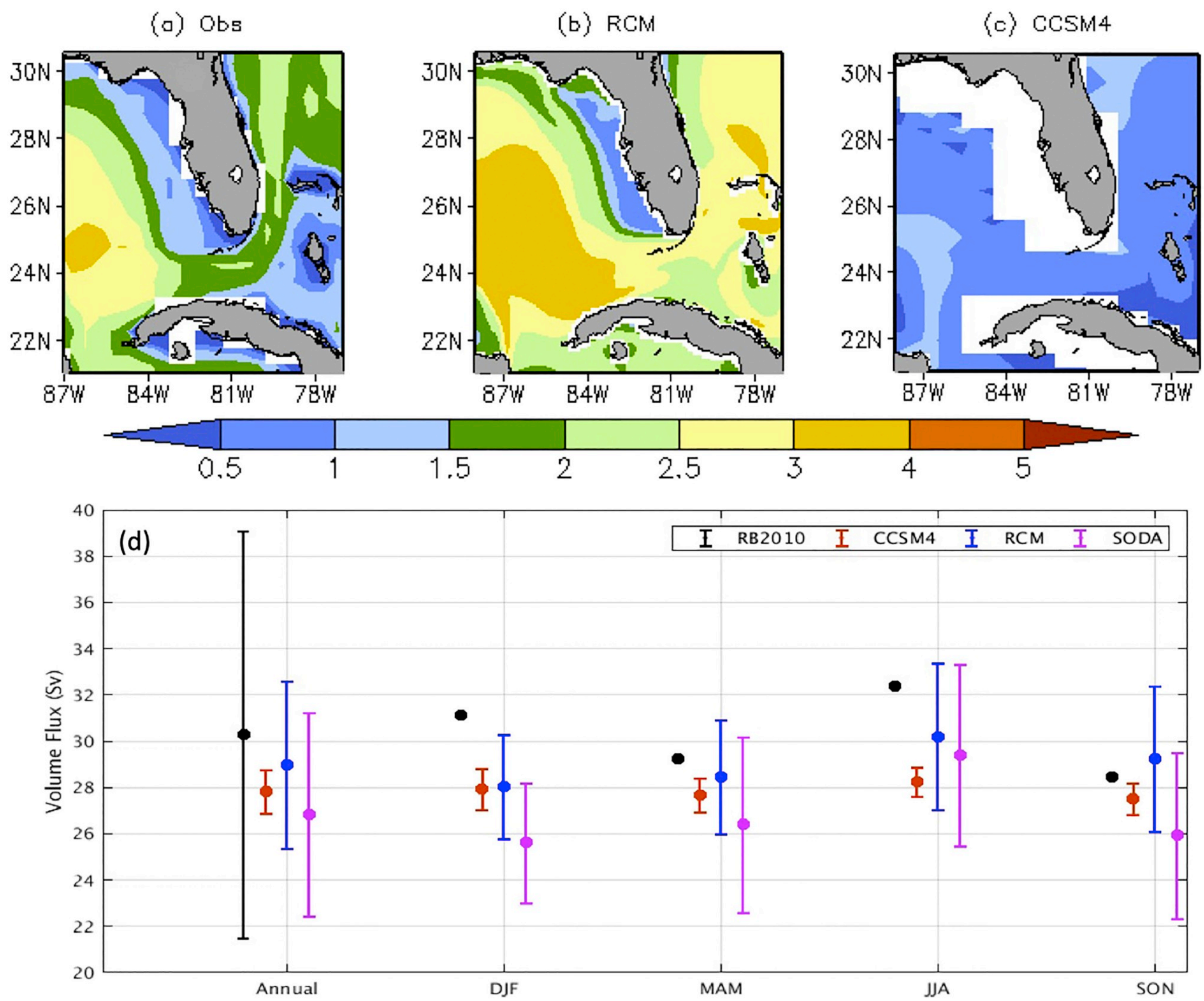

Fig. 3. The annual mean surface eddy kinetic energy plotted on a log scale with base 10 ($cm^2 s^{-2}$) from a) observations (SODA; see Table 2), b) RCM, and c) CCSM4 20th century simulation. d) The climatological annual and seasonal mean volume flux (Sv = $10^6 m^3 s^{-1}$) through the Yucatan Channel are displayed by the filled circles. The whiskers in panel (d) about the filled circles indicate the corresponding standard deviation. The standard deviation of the seasonal mean values from RB2010 was not available.

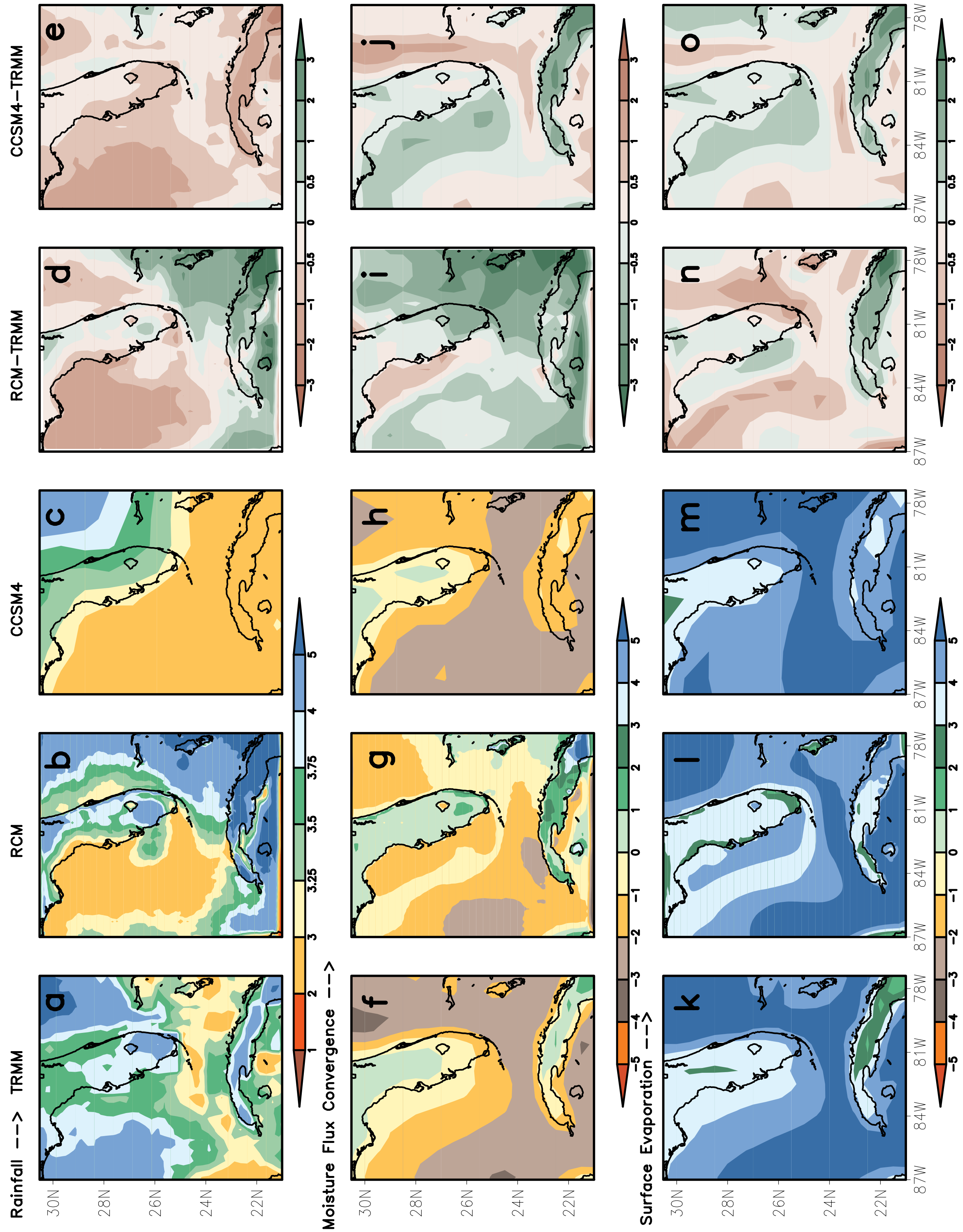
Rainfall --> TRMM
RCM
CCSM4
RCM−TRMM
CCSM4−TRMM
Moisture Flux Convergence -->
Surface Evaporation -->
a
b
c
d
e
f
g
h
i
j
k
l
m
n
o
30N
28N
26N
24N
22N
87W
84W
81W
78W

Fig. 4. The annual mean climatological rainfall (mmday^{-1}) from a) observations (TRMM; see Table 2), b) RCM, and c) CCSM4 20th century simulation. The corresponding systematic errors of rainfall from d) RCM, and e) CCSM4 simulations. Similarly, the annual mean climatological moisture flux convergence from f) observations (MERRA2; see Table 2), g) RCM, and h) CCSM4 20th century simulation. The corresponding systematic errors of moisture flux convergence from i) RCM, and j) CCSM4 simulations. The annual mean climatological surface evaporation from k) observations (MERRA2), l) RCM, and m) CCSM4 20th century simulation. The corresponding systematic errors of surface evaporation from n) RCM, and o) CCSM4 simulations.

that could still be used to evaluate the models. The low values of the surface eddy kinetic energy in CCSM4 indicate that the Loop Current is rather dormant in terms of the lack of eddy activity. The robust circulation of the Loop Current often experiences destabilization from combined barotropic and baroclinic instability that leads to eddy shedding and an increase in the surface eddy kinetic energy (Cherubin et al., 2005; Chérubin et al., 2006). This process of eddy shedding is considered to be vital for heat transport across the western GoM (Chang and Oey, 2010; Misra et al., 2016).

Fig. 3d shows that the climatological annual mean discharge through the Yucatan Channel is about 30Sv from field measurements with a standard deviation of 8.8Sv (Rousset and Beal, 2010). The RCM simulation is closest to this value followed by that of CCSM4 and then SODA reanalysis (Fig. 3d). The seasonal cycle of the discharge through the Yucatan Channel is characterized by a maximum in boreal summer season and preceded and followed in the spring and fall seasons by a minimum (Rousset and Beal, 2010; Fig. 3d), respectively. This is also observed in the RCM simulation and in the SODA reanalysis but this seasonal cycle is rather muted in the CCSM4 simulation (Fig. 3d).

In light of the cable measurements reported in several other studies (Sheinbaum et al., 2002; Candela et al., 2003; Rousset and Beal, 2010; Athie et al., 2015), the inadequacies of the SODA reanalysis should be highlighted with respect to the Loop Current. The SODA reanalysis displays low mean flow and the weak standard deviation of the discharge of the Loop Current through the Yucatan Channel (Fig. 3d). In addition, SODA reanalysis also underestimates the mean flow through the Florida Straits, although its variability is slightly overestimated (not shown). SODA reanalysis, in the absence of observations, fills the data with the model predicted values, which manifests in showing the errors of the model in such regions. The Loop Current is one such data void region.

However, the cable measurements or ship data for the Loop Current region is also deficient. It is available sporadically for limited duration (Sheinbaum et al., 2002; Candela et al., 2003; Rousset and Beal, 2010; Athie et al., 2015), often covered under some temporally limited field campaigns, which is not sufficient to robustly estimate the variability of the Loop Current. Athie et al. (2015) report that there is disparity of over 10% in the volume flux through the Yucatan Channel from several of the non-overlapping observing periods of earlier field campaigns owing largely to interannual variations. Notwithstanding these limitations of the verification data, the RCM simulation shows a significant improvement of the Loop Current simulation over CCSM4, both in terms of the mean flow and its variability through the Yucatan Channel in comparison to the field measurements in Rousset and Beal (2010).

3.1.2. Surface water budget

The surface water budget of precipitation, moisture flux convergence and surface evaporation are shown in Fig. 4. In the observations, the terrestrial region of south Florida receives slightly more rainfall than rest of PF (Fig. 4a). Furthermore, parts of the region over the Loop Current receive less rainfall than the northeast part of the GoM and the western Atlantic Ocean included in the domain (Fig. 4a). However, the contrast between land and ocean is apparent in Fig. 4f, which shows that the oceanic regions have predominantly moisture flux divergence, while the terrestrial part displays convergence with the exception of south Florida that shows some moisture flux divergence. In contrast, nearly across the regional domain the oceanic evaporation exceeds that over PF (Fig. 4k). In essence, the terrestrial precipitation is sustained by moisture flux convergence and surface evaporation, while the oceanic precipitation in the domain is exclusively sustained by surface evaporation and weakened by moisture flux divergence (Fig. 4a, f, and k).

These features of climate over the terrestrial and oceanic regions of PF region are largely simulated in the RCM with more rain in terrestrial Florida (Fig. 4b), moisture flux divergence and convergence in the oceanic and terrestrial regions of the regional domain (Fig. 4g) respectively. Furthermore, the surface evaporation is stronger in the ocean regions (Fig. 4l). There are however differences from observations with especially the dry bias in the GoM and western Atlantic Ocean and the wet bias along the southern and eastern boundary of the domain being most apparent in the RCM simulation (Fig. 4e). The systematic precipitation errors of the RCM simulation over terrestrial PF is comparably far less (Fig. 4e). The mean moisture flux convergence of the RCM (Fig. 4g) is quite similar to the corresponding observed field (Fig. 4f) with the exception of the southeastern part of the domain where the former displays an excess (Fig. 4i). The surface evaporation in the RCM shows a positive bias in the coastal oceans over western Florida Shelf and over Cuba (Figs. 4l and n).

In comparison, the CCSM4 simulation shows a large-scale pattern of precipitation that increases from the southwest to the northeast corner of the domain (Fig. 4c) unlike the observations (Fig. 4a). The CCSM4 simulation displays an overall dry bias across the domain including that over terrestrial PF (Fig. 4e). The moisture flux convergence in the CCSM4 simulation (Fig. 4h) however shows a similar pattern as observations with convergence over terrestrial regions and divergence over the oceanic parts of the domain (Fig. 4h) with a large bias of opposite signs on either side of PF (Fig. 4j). The surface evaporation in the CCSM4 also follows a similar pattern of more evaporation over the oceanic than the terrestrial regions of the domain (Fig. 4m) but with a large positive bias over the WFS (Fig. 4o).

The systematic errors of the hydrological budget of the RCM (Fig. 4d, i, n) shows the prevalence of the boundary errors of the RCM simulation in the southern and eastern boundaries of the domain where there is an excess wet bias (Fig. 4d) largely reinforced by the moisture flux convergence (Fig. 4i). These errors are unfortunately very difficult to avoid because of the ill posed boundary value problem in regional models (Misra, 2007). Despite this issue, the RCM simulation does seem to preserve and simulate the observed fine scale structures in the patterns of precipitation (Fig. 4b), moisture flux convergence (Fig. 4g), and surface evaporation (Fig. 4l) over PF in comparison to the corresponding figures from the simulation of the CCSM4 (Fig. 4c, h, and m). The systematic errors of precipitation, area averaged in the form RMS errors and bias for the three regions of WFS, PF, and FEW in Table 3 for precipitation clearly indicate the improvement of RCM over CCSM4, except over the FEW region where the number of grid points in CCSM4 to evaluate is far less than that in RCM.

3.2. Simulation of the future climate (2041–2060)

3.2.1. Surface water budget

Fig. 5 shows the difference of the projected mean from the corresponding mean of the current climate in relation to the terms of the surface water budget from the RCM and CCSM4 simulations. A significant difference is apparent in the projected rainfall anomalies between the two model simulations (Fig. 5a and d). The RCM simulation indicates an overall reduction of rainfall in the future climate with the exception over WFS and along the eastern and southern edge of the domain (Fig. 5a). The RCM displays uniform reduction of the future rainfall over terrestrial regions of PF (Fig. 5a). On the other hand, the CCSM4 simulation projects a moderate change with some relative decrease and increase in the southern and northern parts of the domain compared to the current climate (Fig. 5d), respectively. In fact, Fig. 5d shows that the CCMS4 projects an overall relative increase of future precipitation over terrestrial PF except near the southern tip. The RCM projection displays a relative decrease in the moisture flux convergence across the domain with the exception along the eastern and southern edge of the regional domain (Fig. 5b). In contrast, the CCSM4 projection shows a comparative decrease and increase in moisture flux convergence over oceanic and terrestrial PF parts of the domain (Fig. 5e), respectively. Similarly, the surface evaporation shows a tendency to comparatively increase and decrease in the oceanic and terrestrial parts of the RCM domain (Fig. 5c), respectively. It is interesting to note the contrasting change in evaporation between PF and WFS in the RCM simulations (Fig. 5c). In contrast, the CCSM4 projection displays an overall moderate increase in surface evaporation with a marginal decrease over southern Florida in the future relative to current climate (Fig. 5f).

3.2.2. Upper ocean climate

The SST's in the future climate simulation of RCM (Fig. 6a) and CCSM4 (Fig. 6d) show higher values relative to the current climate. The RCM displays considerably higher values of SST in the future climate, especially along the WFS relative to CCSM4. This is in part because of the resolution of the coastal bathymetry in the RCM that reduces the depth of the ocean considerably over the shelf and thereby making it respond to changes in the atmospheric heat flux. The depth of the 26 °C isotherm shows a deepening in the future climate of the RCM simulation (Fig. 6b) and the CCSM4 simulation (Fig. 6e), especially along the Loop Current, with the former suggesting slightly less than the latter. Similarly, there is further deepening of the 20 °C isotherm in both the RCM (Fig. 6c) and CCSM4 (Fig. 6f) simulations.

3.2.3. Atmospheric fluxes

We show the annual mean climatology of surface net heat flux (Fig. 7a) and the corresponding components including net surface shortwave (Fig. 7b), net surface longwave (Fig. 7c), latent heat flux (Fig. 7d) and sensible heat flux (Fig. 7e) from the RCM 20th century simulation. It may be noted that positive values of the flux in Fig. 7a-e suggest that flux is downward towards the ocean and negative fluxes mean that the flux is upward towards the atmosphere from the ocean. Therefore in Fig. 7a, the net heat flux is marginally upward in PF, while over the WFS it is downward and along the Loop Current it is largely upward. Fig. 7b clearly shows that the net surface shortwave flux is downward and significantly larger over the oceans compared to that over PF. This shortwave flux is compensated by the upward fluxes of net longwave (Fig. 7c), latent heat flux (Fig. 7d) and sensible heat flux (Fig. 7e), with the sensible heat flux being much larger over PF than the surrounding oceans, contrary to both surface longwave and latent heat flux.

The projected change of the net heat flux from the RCM in Fig. 7f suggests that in the future climate, there is marginal decrease of the upward flux over PF, slightly less downward flux over WFS and far less upward flux over the Loop Current and over the FEW regions. In the subsequent Fig. 7g-j, we computed the Fractional Change (FC) given by:

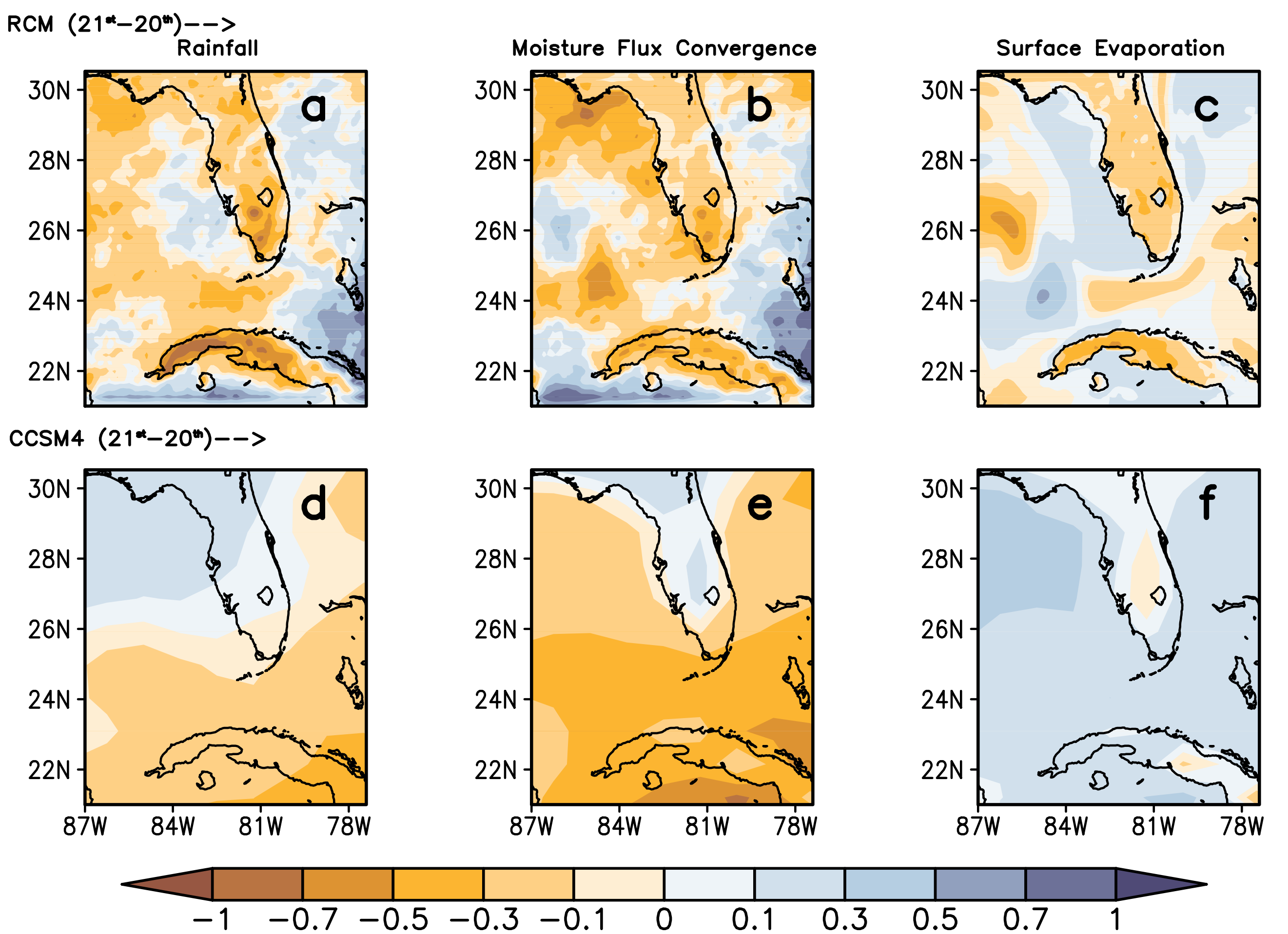

Fig. 5. The projected annual mean climatological (2041–2060) difference from the mean current climate (1986–2005) for (a, d) rainfall ($mmday^{-1}$), (b, e) moisture flux convergence ($mmday^{-1}$), and (c, f) surface evaporation ($mmday^{-1}$) from (a, b, c) RCM and (d, e, f) CCSM4 simulations.

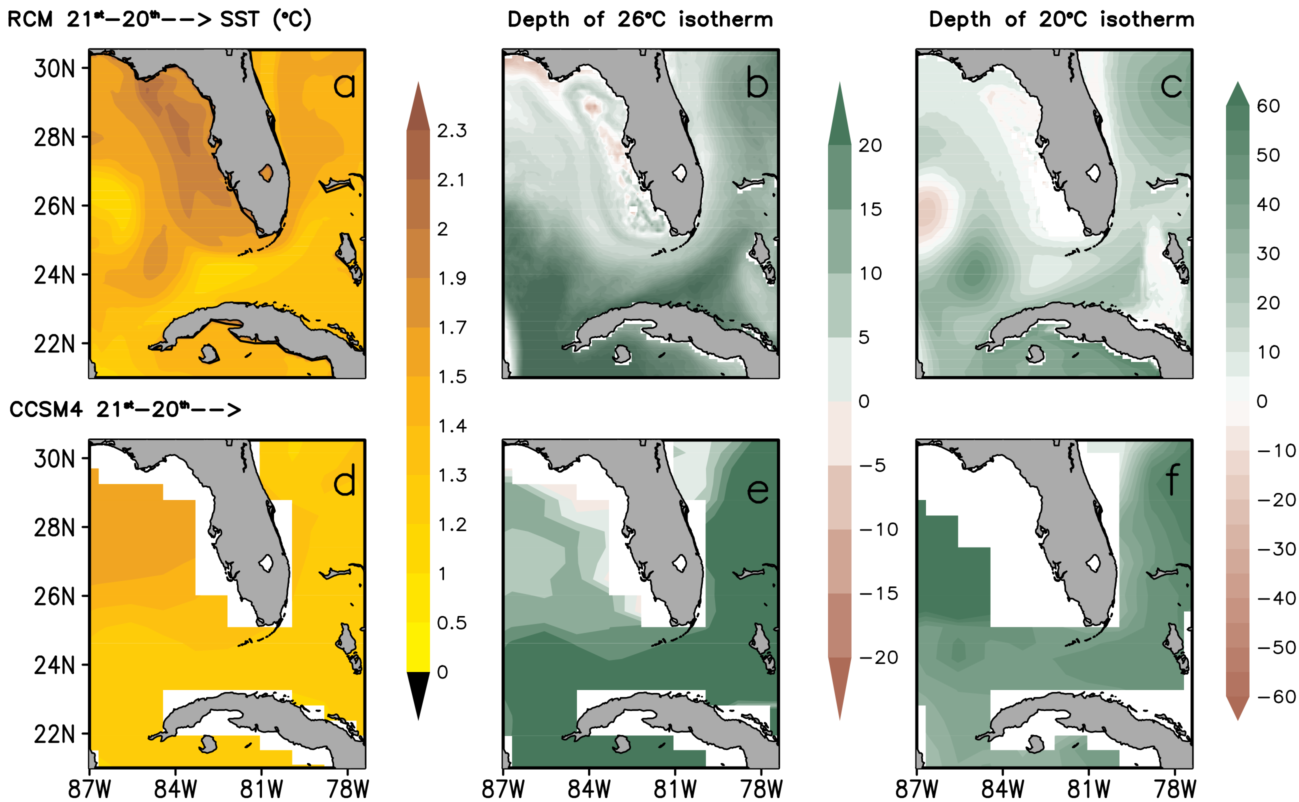

Fig. 6. The projected annual mean climatological (2041–2060) difference from the mean current climate (1986–2005) for (a, d) SST (°C), (b, e) depth of the 26 °C isotherm, and (c, f) depth of the 20 °C isotherm (in meters).

$$FC = \frac{a_i^{21st} - a_i^{20th}}{N^{21st} - N^{20th}} \tag{1}$$

Where, $a_i^{21st}$and a_i^{20th}refer to the i$^{\text{th}}$ flux component (shortwave, longwave, latent, and sensible heat flux) of 21st and 20th century annual mean climatology of the RCM simulations respectively. Similarly, N^{21st} and N^{20th} refer to the annual mean climatology of the net heat flux from the 21$^{\text{st}}$ and 20th century simulations of the RCM respectively. Therefore, FC represents the fractional projected change of a given component of the surface flux relative to the projected change in the net surface heat flux from the RCM simulations. It may be noted that a negative sign in FC would mean that the projected change in the flux component is contrary to net heat flux change. So, over the WFS, to a large extent, there is a projected increase in the downward shortwave flux (Fig. 7g), a projected decrease in the upward longwave flux (Fig. 7h), a projected increase in the upward latent heat flux (Fig. 7i), and a projected decrease in the upward sensible heat flux (Fig. 7j) that results in a net, projected decrease of the downward net heat flux (Fig. 7f). The changes in shortwave flux (Fig. 7g) and latent heat flux (Fig. 7i) are however dominating over the WFS. Similarly, over the PF, the marginal projected decrease in the upward net heat flux is a result of the projected increase in the shortwave flux (Fig. 7g), projected increase in the upward longwave flux (except over southwest Florida; Fig. 7h), a projected decrease in the latent heat flux (Fig. 7i) and a projected increase in the sensible heat flux (Fig. 7j). Similarly, over the Loop Current region, the projected net decrease in the upward net heat flux (Fig. 7f) results from a projected increase in the downward shortwave flux (Fig. 7g), a projected decrease in the upward long wave flux (Fig. 7h), a projected decrease in the upward latent heat flux (Fig. 7i) and a projected decrease in the upward sensible heat flux (Fig. 7j). The magnitude of the fractional change in all of these regions suggest that the projected changes in shortwave flux and latent heat flux are dominating and to a large extent compensatory to each other, except over PF where the changes in sensible heat flux term is also dominating.

3.2.4. Atmospheric clouds

The high (Fig. 8a, d), middle (Fig. 8b and e), and low (Fig. 8c and f) cloud fractions from 20$^{\text{th}}$ and 21st century simulations of the RCM clearly indicate that low cloud fraction dominates the cloud cover with the least contribution from the high clouds, both over PF and the surrounding oceans. Furthermore, the projected change from the RCM clearly indicates that the future climate will have less middle (Fig. 8h) and low (Fig. 8i) clouds both over the oceans and PF, while there is a modest increase in the high cloud fraction over parts of WFS (Fig. 8g). These projected changes in clouds are consistent with the corresponding projected change in rainfall (Fig. 5a) and in surface fluxes (Figs. 7f-j). For example, over PF the projected increase in shortwave flux (Fig. 7g) and the projected increase in upward longwave flux (Fig. 7h) is consistent with a future drier climate over PF (Fig. 5a) and reduction of the middle (Fig. 8h) and low (Fig. 8i) clouds. Similarly, the future increase in the annual mean rainfall over the WFS (Fig. 5a) is consistent with projected reduction of shortwave flux (Fig. 7g), projected increase of longwave flux (Fig. 7h) and projected increase in high cloud fraction (Fig. 8g).

3.2.5. The loop current system

An important feature of the RCM simulation is that the ocean surface of the domain warms considerably in the future climate (Fig. 6a). Some of the excess warming in the RCM (Fig. 6a) can also be explained by the convergence of the heat flux anomalies in the sub-surface ocean. Ocean heat flux through a passage like the Yucatan Channel or the Florida Straits (HF) is given by:

$$HF = \int_A \vec{V}\theta C_w \rho_w dA \tag{2}$$

where, A is the cross-sectional area of the channel or strait, C_w and ρ_w are heat capacity and density of seawater, and θ is the potential temperature. The convergence of HF in the GoM (C) is then given by the difference in the values of HF through the Yucatan Channel (HF_{YC}) and

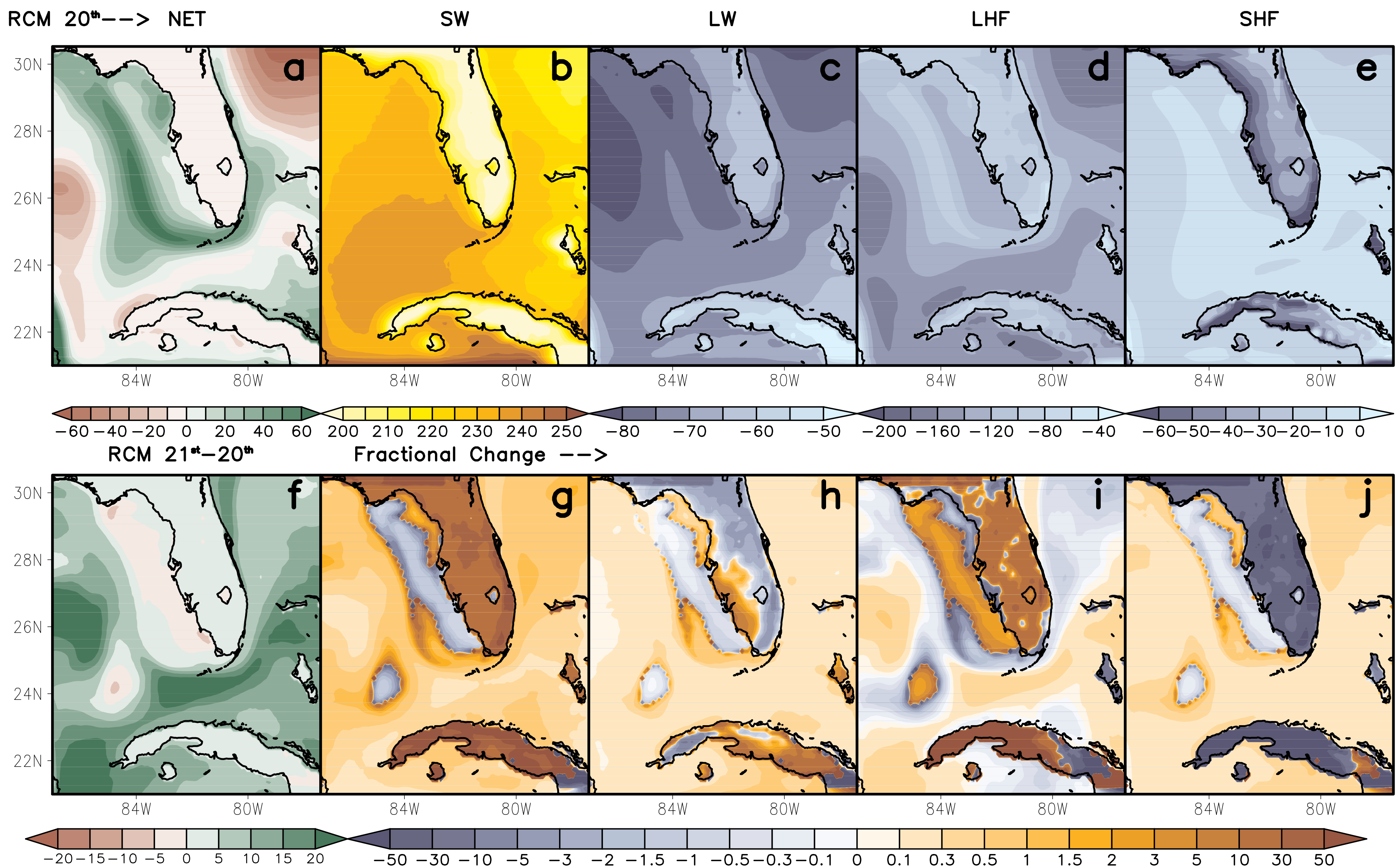

Fig. 7. The annual mean climatology of surface a) net heat flux, b) short wave, c) long wave, d) latent heat, and e) sensible heat flux from the 20th century RCM simulation. The positive sign of the fluxes mean that it is directed from the atmosphere into the ocean (downward) while negative sign suggests that the flux is directed from the ocean into the atmosphere (upward).The corresponding projected change in the f) surface net heat flux and the fractional projected change (see text) of g) short wave, h) long wave, i) latent heat, and j) sensible heat flux. The units in Fig. 7a-f is in Wm^{-2} and that in Fig. 7g-j is unitless.

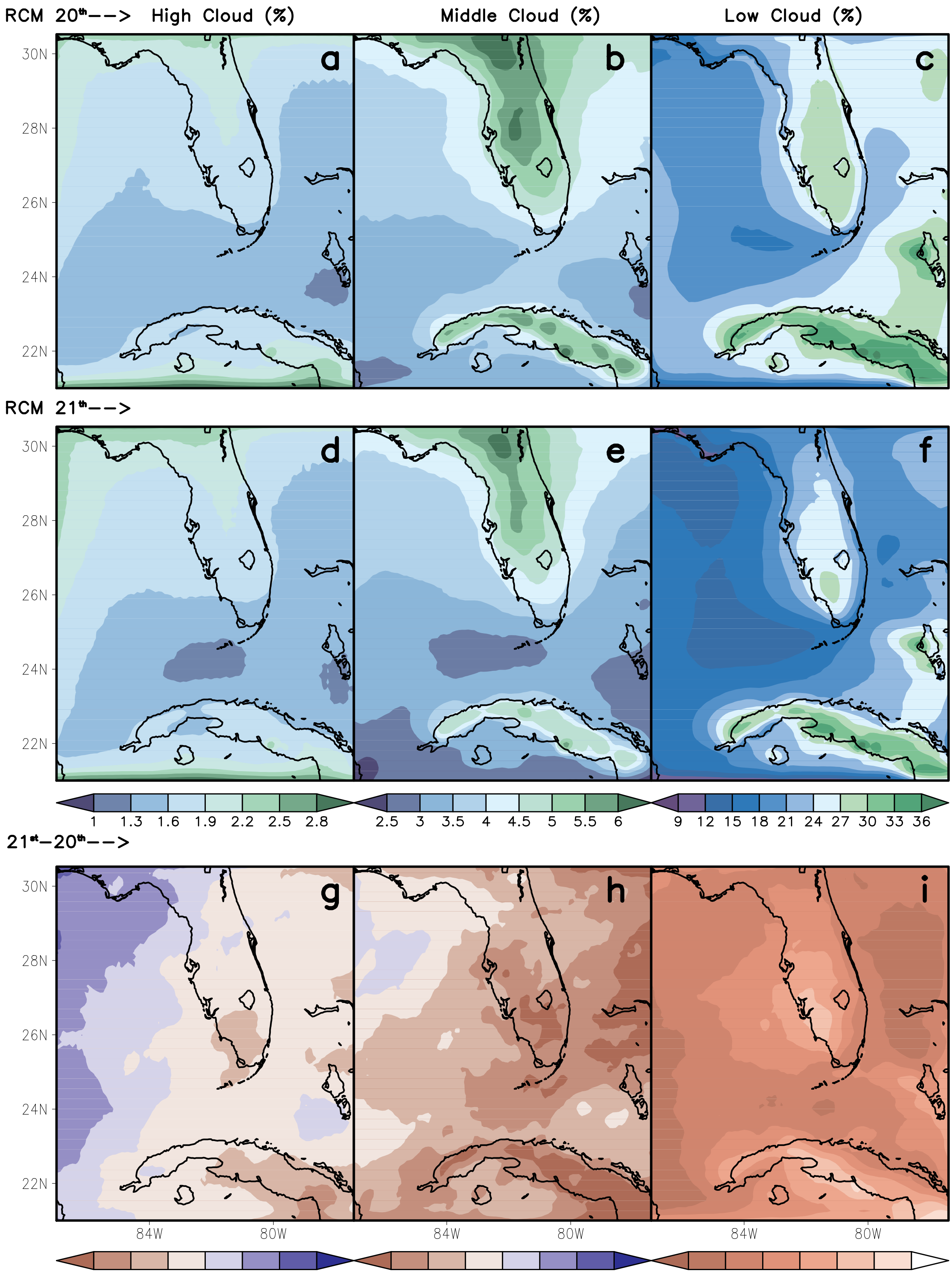

Fig. 8. The 20th century mean (1986–2005) climatological annual mean a) high, b) middle, and c) low cloud fraction. Similarly, the 21st century mean (2041–2060) annual mean climatological d) high, e) middle, and f) low cloud fraction from the RCM simulation. The corresponding differences (21st century-20th century mean) are shown for g) high, h) middle, and i) low cloud fraction. The cloud fraction is expressed in percent.

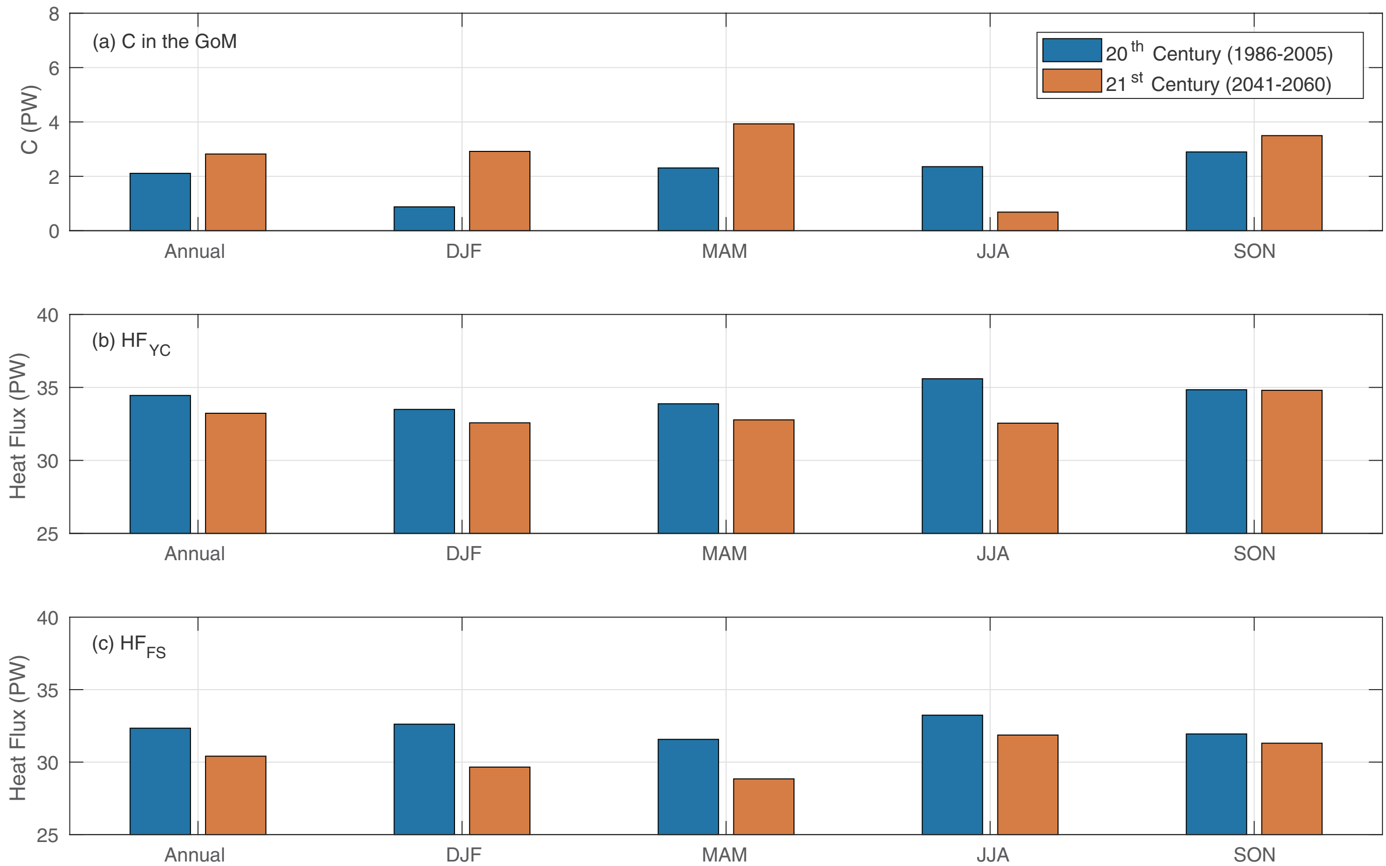

Fig. 9. The climatological annual and seasonal mean a) convergence (C from Eq. 3 of text) of ocean heat flux in the GoM, b) HF_{YC} (see text) and c) HF_{FS} (see text; computed between Florida and Cuba at 80.031°W) from the RCM simulation. The units are PetaWatts (PW).

the Florida Strait (HF_{FS}). Mathematically,

$$C = HF_{YC} - HF_{FS} \quad (3)$$

The convergence of HF, C, for the 20th and 21st century simulations from the RCM is shown in Fig. 9. It is apparent that the annual mean convergence (C) in RCM has increased in the future simulation relative to the current climate simulation. This is from the corresponding slowing of the heat transport across the Loop Current as illustrated by the reduction in HF_{YC} and HF_{FS}, with a slightly larger reduction in the latter. Liu et al. (2012) concluded similarly from downscaling of just the ocean component of the CMIP5 models that despite a weakening of the Loop Current in the future climate, the ocean heat content continues to rise in the projected climate owing to anomalous advective heat flux convergence. The seasonal variations of this change indicate that C exhibits the smallest projected decrease in the boreal summer (June–-July-August [JJA]) followed by the winter (December–January-February [DJF]) seasons. The largest decrease in C happens in the boreal spring (March–April-May [MAM]) followed by the fall (September–-October-November [SON]) seasons. The heat transports HF_{YC} and HF_{FS} also show similar projected changes, with the latter showing slightly larger projected decrease than the former in the MAM season. In the boreal summer season, however, when the projected decrease in C is the least in the year shows that the projected decrease in HF_{YC} is more than HF_{FS}. In other words, the RCM projections indicate that the projected convergence of the heat flux anomalies in the Gulf of Mexico by the Loop Current is maximum and minimum when the seasonal cycle of the volume flux through the Yucatan Channel is minimum and maximum, respectively.

4. Discussion

Several other climate projection studies have been conducted with regional coupled ocean-atmosphere models over other domains (e.g., Somot et al., 2008; Li et al., 2012; Dubois et al., 2012; Gualdi et al., 2013). They find that inclusion of air-sea coupling has a profound impact on the climate projections in the regional models. For example, Somot et al. (2008) found that inclusion air-sea coupling in the regional model significantly amplified the climate change signal over large parts of Europe relative to the projection from its uncoupled, atmosphere only regional model simulation. They found that the response of the climate change forcing of the Mediterranean Sea was primarily responsible for the differing result between the coupled and uncoupled versions of the regional model projections. In contrast, Li et al. (2012) found that the projected warming over California coast was weaker from the inclusion of air-sea coupling as the regional model was able to resolve the coastal upwelling far better than the driving global model. The RCM projections in this study show that the coastal oceans around PF warm significantly more and dries over PF than the CCSM4 projections.

The seasonal modulation of the Loop Current system by the climate change forcing is also observed in the RCM simulation (Fig. 9). This points to the additional importance of using high resolution coupled models for projection of climate over this region because of the potential influence of this current system on the hydroclimate over PF (Misra and Mishra, 2016) and the heat content in the oceans surrounding PF, which can dictate the intensity of the Atlantic tropical cyclones (Rappaport and Franklin, 2010). It is not clear if similar results as those presented here for the RCM could be achieved by using a global model at a similar resolution. There are some recent global modeling studies, however, that have been run with comparable resolution for the ocean component of the global climate model (as the RCM in this study) and the coupled atmospheric component model being coarser in resolution, which suggest that the resolved mesoscale ocean eddies in such global models have an impact on the surface turbulent flux, overlying atmospheric circulation and convective precipitation (Kirtman et al., 2012; Putrasahan et al., 2017).

The ocean downscaled projections in Liu et al. (2015) also show significant warming in the WFS. Morey et al. (2017) suggest that over the WFS, the surface ocean circulation is weak and detached from the Loop Current system, which further suppresses the mixing with deeper cooler waters. Therefore, they argue that there is no mechanism in the WFS to offset the increased surface heating in a future warming scenario.

This study can be further expanded to examine in more detail the projected seasonal changes by using a larger ensemble of high resolution RCMs to account for model uncertainty. Furthermore, as mentioned earlier in Section 2, the domain of the RCM could be further expanded westward, to allow the full resolution of the Loop Current in the regional domain. As such with the given domain the volume flux through the Yucatan Channel is influenced by the lateral boundary forcing. Therefore, any rectification impact of the RCM on the global model simulation would be limited to some extent by this choice of the regional domain.

5. Conclusions

In this paper, we have downscaled a global model (CCSM4) simulation for current (1986–2005) and future (2041–2060) climate to 10 km grid spacing using a regional coupled ocean-atmosphere climate model (RCM). This dynamic downscaling effort is different from a more conventional atmosphere only or ocean only downscaling of such global model simulations because coupled air-sea interactions of the RCM could have a mutual rectification impact on the evolving high resolution regional climate system. The evidence for such rectification is seen in this study both in the ocean and in the atmosphere of the RCM. For example, we see moderate improvements in the ocean circulations, upper ocean heat content, SST's and in the surface hydrological components of the atmosphere. However, some of the large-scale biases in the CCSM4 perpetuates in the RCM simulation and also has a tendency to further deteriorate the bias (e.g. dry bias over northeast GoM). Additionally, the ill posed boundary of the RCM continues to be a vexing issue. Nonetheless, the overall improvements in the climatology of the oceanic and atmospheric components of the regional climate system around PF in the RCM relative to CCSM4 is encouraging and suggests the benefits of downscaling. It should however be noted that the differences between the RCM and CCSM4 cannot be totally attributed to the differences in the resolution of the two models as there are significant differences in the model physics and formulations.

The projected mean climate of the RCM shows an overall drying across the regional domain contrary to CCSM4 that shows a slight increase in rainfall over northern parts of the domain. This moderate increase of rainfall in future climate in CCSM4 is largely sustained by a corresponding increase in evaporation across the domain and a moderate increase in terrestrial moisture flux convergence. However, in the RCM, despite an increase in evaporation over some parts of the neighboring oceans including the WFS, PF displays drying in the future climate as a result of a reduction of moisture flux convergence and as well as reduction of local terrestrial surface evaporation. The RCM shows a tendency to decrease the low-level clouds that increases the net heat flux across the regional domain. With shallower coastal oceans resolved in the RCM, the excess atmospheric heat flux warms the coastal oceans further in the RCM than in the CCSM4. The increase in atmospheric convection in the future climate simulation of the RCM over the WFS results in an increase in the high cloud fraction resulting in the slight reduction of downward shortwave flux and a net reduction of heat flux entering the ocean surface. However, the RCM also indicates a relative weakening of the Loop Current in the future climate, consistent with findings of some of the previous studies (Liu et al., 2015). The RCM also projects a convergence of the ocean heat flux in the GoM from this slowing of the Loop Current, which leads to warming of the surface and sub-surface ocean in the region in the future projections of the RCM simulation.

This study does highlight the importance of downscaling to higher resolution, especially for a region like PF that has robust circulation features in the ocean, which can influence the overlying atmosphere. Although one cannot be totally conclusive by downscaling just one ensemble member of one global model even when mean climate is being assessed as it has been repeatedly shown that regionalization of climate change projections often raise the uncertainty (Jacob et al., 2007; Christensen et al., 2008; Mearns et al., 2012), the paper does lay ground for a serious effort to downscale a larger ensemble of global models for a region like Florida.

Acknowledgements

We thank Dr. Gokhan Danabasoglu of NCAR for sharing the CCSM4 bathymetry data and Dr. Robert E. Hart of Florida State University in helping with Fig. 1. The authors would like to acknowledge the editorial assistance of Mrs. Tracy Ippolito of the Center for Ocean-Atmospheric Prediction Studies, Florida State University. This work was also supported by NOAA grant NA12OAR4310078 and the South Florida Water Management District (PO 039231). The supercomputing facility provided by XSEDE under Grant ATM10010 was used to complete the model integrations used in this study. The authors have no conflicts of interest to declare.

References

Adler, R.F., Huffman, G.J., Bolvin, D.T., Curtis, S., Nelkin, E.J., 2000. Tropical rainfall distributions determined using TRMM combined with other satellite and rain gauge information. J. Appl. Meteorol. 39 (12), 2007–2023.

Alpert, J., Kanamitsu, M., Caplan, P., Sela, J., White, G., 1988. Mountain induced gravity wave drag parameterization in the NMC medium-range forecast model. In: Conference on Numerical Weather Prediction, 8th, Baltimore, MD, pp. 726–733.

Athie, G., Sheinbaum, J., Leben, R., Ochoa, J., Shannon, M.R., Candela, 2015. Interannual variability in the Yucatan Channel flow. Geophys. Res. Lett. 42, 1496–1503. https://doi.org/10.1002/2014GL062674.

Campbell, J.D., Taylor, M.A., Stephenson, R.S., Watson, R.A., Whyte, F.S., 2011. Future climate of the Caribbean from a regional climate model. Int. J. Climatol. https://doi.org/10.1002/joc.2200.

Candela, J., Tanahara, S., Crepon, M., Barnier, B., Sheinbaum, J., 2003. Yucatan channel flow: observations versus CLIPPER ATL6 and MERCATOR PAM models. J. Geophys. Res. 108 (C12), 3385–3408. https://doi.org/10.1029/2003jc001961.

Carter LM, Jones JW, Berry L, Burkett V, Murley JF, Obeysekera J, Schramm PJ, Wear D (2014) Ch. 17: Southeast and the Caribbean. Climate Change Impacts in the United States: The Third National Climate Assessment, J. M. Melillo, Terese (T.C.) Richmond, and G. W. Yohe, Eds., U.S. Global Change Research Program, 396–417. doi:https://doi.org/10.7930/J0N-P22CB.

Carter, L., A. Terando, K. Dow, K. Hiers, K.E. Kunkel, A. Lascurain, D. Marcy, M. Osland, and P. Schramm, 2018: Southeast. In Impacts, Risks, and Adaptation in the United States: Fourth National Climate Assessment, Volume II [Reidmiller, D.R., C.W. Avery, D.R. Easterling, K.E. Kunkel, K.L.M. Lewis, T.K. Maycock, and B.C. Stewart (Eds.)]. U. S. Global Change Research Program, Washington, DC, USA, pp. 743–808. doi:https://doi.org/10.7930/NCA4.2018.CH19.

Carton, J.A., Giese, B.S., 2008. A reanalysis of ocean climate using Simple Ocean Data Assimilation (SODA). Mon. Weather Rev. 136 (8), 2999–3017.

Chang, Y.L., Oey, L.Y., 2010. Why can wind delay the shedding of Loop Current eddies? J. Phys. Oceanogr. 40 (11), 2481–2495.

Cherubin, L.M., Sturges, W., Chassignet, E.P., 2005. Deep flow variability in the vicinity of the Yucatan Straits from a high-resolution numerical simulation. Journal of Geophysical Research: Oceans. 110 (C4).

Chérubin, L.M., Morel, Y., Chassignet, E.P., 2006. Loop current ring shedding: the formation of cyclones and the effect of topography. J. Phys. Oceanogr. 36 (4), 569–591.

Chou, M.D., Lee, K.T., 1996. Parameterizations for the absorption of solar radiation by water vapor and ozone. J. Atmos. Sci. 53, 1203–1208.

Chou, M.D., Suarez, M.J., 1994. An efficient thermal infrared radiation parameterization for use in general circulation models. National Aeronautics and Space Administration. Goddard Space Flight Center. Tech. Memo. 104606 (3), 85.

Christensen, J.H., Carter, T.R., Rummukainen, M., Amanatidis, G., 2007. Evaluating the performance and utility of regional climate models: the PRUDENCE project. Clim. Chang. 81, 1–6.

Christensen, J.H., Boberg, F., Christensen, O.B., Lucas-Picher, P., 2008. On the need for

bias correction of regional climate change projections of temperature and precipitation. Geophys. Res. Lett. 35 (20).
Cubasch, U., Waszkewitz, J., Hegerl, G., Perlwitz, J., 1995. Regional climate changes as simulated in time-slice experiments. Clim. Chang. 31 (2–4), 273–304.
Denis, B., Laprise, R., Caya, D., Côté, J., 2000. Downscaling ability of one-way nested regional climate models: the Big-Brother Experiment. Clim. Dyn. 18 (8), 627–646.
Donlon, C.J., Martin, M., Stark, J.D., Roberts-Jones, J., Fiedler, E., Wimmer, W., 2011. The operational sea surface temperature and sea ice analysis (OSTIA). Remote Sens. Environ. 116, 140–158. https://doi.org/10.1016/j.rse.2010.10.017.
Douglas, B.C., Kearney, M.S., Leatherman, S.R., 2001. Sea Level Rise: History and Consequences. Academic Press.
Dubois, C., Somot, S., Calmanti, S., Carillo, A., Déqué, M., Dell'Aquilla, A., Elizalde, A., 2012. Future projections of the surface heat and water budgets of the Mediterranean sea in an ensemble of coupled atmosphere-ocean regional climate models. Climate Dynamics. 39, 1859–1884.
Ek, M.B., Mitchell, K.E., Lin, Y., Rogers, E., Grunmann, P., Koren, V., Gayno, G., Tarpley, J.D., 2003. Implementation of Noah land surface model advances in the National Centers for Environmental Prediction operational mesoscale Eta model. Journal of Geophysical Research: Atmospheres 108 (D22).
Gent, P.R., Danabasoglu, G., Donner, L.J., Holland, M.M., Hunke, E.C., Jayne, S.R., Lawrence, D.M., Neale, R.B., Rasch, P.J., Vertenstein, M., Worley, P.H., 2011. The community climate system model version 4. J. Clim. 24 (19), 4973–4991.
Giorgi, F., Jones, C., Asrar, G.R., 2009. Addressing climate information needs at the regional level: the CORDEX framework. World Meteorological Organization (WMO) Bulletin 58 (3), 175.
Glazer, R., Misra, V., 2018. Ice versus liquid water saturation in simulations of the Indian summer monsoon. Clim. Dyn. https://doi.org/10.1007/s00382-018-4116-4.
Gregory, J.M., et al., 2005. A model intercomparison of changes in the Atlantic thermohaline circulation in response to increasing atmospheric CO2 concentration. Geophys. Res. Lett. 32, L12703.
Gualdi, S., Somot, S., Li, L., et al., 2013. The CIRCE simulations: regional climate change projections with realistic representation of the Mediterranean Sea. Bull. Amer. Soc. 94, 65–81.
Haidvogel, D.B., Arango, H.G., Hedstrom, K., Beckmann, A., Malanotte-Rizzoli, P., Shchepetkin, A.F., 2000. Model evaluation experiments in the North Atlantic Basin: simulations in nonlinear terrain-following coordinates. Dynamics of atmospheres and oceans 32 (3), 239–281.
Hewitson, B.C., Crane, R.G., 1996. Climate downscaling: techniques and application. Clim. Res. 85–95.
Hong, S.Y., Pan, H.L., 1996. Nonlocal boundary layer vertical diffusion in a medium-range forecast model. Mon. Weather Rev. 124 (10), 2322–2339.
Huffman, G.J., Adler, R.F., Rudolf, B., Schneider, U., Keehn, P.R., 1995. Global precipitation estimates based on a technique for combining satellite-based estimates, rain gauge analysis, and NWP model precipitation information. J. Clim. 8 (5), 1284–1295.
Huffman, G.J., Adler, R.F., Arkin, P., Chang, A., Ferraro, R., Gruber, A., Janowiak, J., McNab, A., Rudolf, B., Schneider, U., 1997. The global precipitation climatology project (GPCP) combined precipitation dataset. Bull. Am. Meteorol. Soc. 78 (1), 5–20.
Jacob, D., Bärring, L., Christensen, O.B., Christensen, J.H., de Castro, M., Deque, M., Giorgi, F., Hagemann, S., Hirschi, M., Jones, R., Kjellström, E., 2007. An inter-comparison of regional climate models for Europe: model performance in present-day climate. Clim. Chang. 81, 31–52.
Juang, H.M., Kanamitsu, M., 1994. The NMC nested regional spectral model. Mon. Weather Rev. 122 (1), 3–26.
Kanamaru, H., Kanamitsu, M., 2007. Scale-selective bias correction in a downscaling of global analysis using a regional model. Mon. Weather Rev. 135 (2), 334–350.
Kanamitsu, M., Yoshimura, K., Yhang, Y.B., Hong, S.Y., 2010. Errors of interannual variability and trend in dynamical downscaling of reanalysis. Journal of Geophysical Research: Atmospheres. 115 (D17).
Kessler, W.S., 1990. Observations of long Rossby waves in the northern tropical Pacific. Journal of Geophysical Research: Oceans. 95 (C4), 5183–5217.
Kirtman, B., Bitz, C., Bryan, F., et al., 2012. Impact of ocean model resolution on CCSM climate simulations. Clim. Dyn. 39, 1303–1328. https://doi.org/10.1007/s00382-012-1500-3.
Laprise, R.R., De Elia, R., Caya, D., Biner, S., Lucas-Picher, P.H., Diaconescu, E., Leduc, M., Alexandru, A., Separovic, L., 2008. Challenging some tenets of regional climate modelling. Meteorog. Atmos. Phys. 100 (1–4), 3–22.
Large, W.G., McWilliams, J.C., Doney, S.C., 1994. Oceanic vertical mixing: a review and a model with a nonlocal boundary layer parameterization. Rev. Geophys. 32 (4), 363–403.
Leipper, D.F., Volgenau, D., 1972. Hurricane heat potential of the Gulf of Mexico. J. Phys. Oceanogr. 2 (3), 218–224.
Li, H., Kanamitsu, M., Hong, S.Y., 2012. California reanalysis downscaling at 10 km using an ocean-atmosphere coupled regional model system. Journal of Geophysical Research: Atmospheres. 117 (D12).
Li, H., Kanamitsu, M., Hong, S.Y., Yoshimura, K., Cayan, D.R., Misra, V., 2014a. A high-resolution ocean-atmosphere coupled downscaling of the present climate over California. Clim. Dyn. 42 (3–4), 701–714.
Li, H., Kanamitsu, M., Hong, S.Y., Yoshimura, K., Cayan, D.R., Misra, V., Sun, L., 2014b. Projected climate change scenario over California by a regional ocean–atmosphere coupled model system. Clim. Chang. 122 (4), 609–619.
Liu Y, Lee SK, Muhling BA, Lamkin JT, Enfield DB (2012) Significant reduction of the Loop Current in the 21st century and its impact on the Gulf of Mexico. J. Geophys. Res. 117, C05039, doi:https://doi.org/10.1029/2011JC007555.
Liu, Y., Lee, S.K., Enfield, D.B., Muhling, B.A., Lamkin, J.T., Muller-Karger, F.E., Roffer, M.A., 2015. Potential impact of climate change on the intra-Americas sea: Part-1. A dynamic downscaling of the CMIP5 model projections. J. Mar. Syst. 148, 56–69.
Marx L (2002) New Calculation of Saturation Specific Humidity and Saturation Vapor Pressure in the COLA Atmospheric General Circulation Model.
Mearns, L.O., Arritt, R., Biner, S., Bukovsky, M.S., McGinnis, S., Sain, S., Caya, D., Correia Jr., J., Flory, D., Gutowski, W., Takle, E.S., 2012. The North American regional climate change assessment program: overview of phase I results. Bull. Am. Meteorol. Soc. 93 (9), 1337–1362.
Meehl GA, et al. (2007) The Physical science basis: Contribution of the working group I to the fourth assessment report of the Intergovernmental Panel on Climate Change (Eds. S. Solomon et al.), Cambridge University Press, 747–845.
Mellor, G.L., Yamada, T., 1982. Development of a turbulence closure model for geophysical fluid problems. Rev. Geophys. 20 (4), 851–875.
Misra, V., 2007. Addressing the issue of systematic errors in a regional climate model. J. Clim. 20 (5), 801–818.
Misra, V., Mishra, A., 2016. The oceanic influence on the rainy season of Peninsular Florida. Journal of Geophysical Research: Atmospheres. 121 (13), 7691–7709.
Misra, V., Mishra, A., Li, H., 2016. The sensitivity of the regional coupled ocean-atmosphere simulations over the Intra-Americas seas to the prescribed bathymetry. Dynamics of Atmospheres and Oceans 76, 29–51.
Misra, V., Mishra, A., Bhardwaj, A., 2017. High-resolution regional-coupled ocean–atmosphere simulation of the Indian Summer Monsoon. Int. J. Climatol. https://doi.org/10.1002/joc5034.
Moorthi, S., Suarez, M.J., 1992. Relaxed Arakawa-Schubert. A parameterization of moist convection for general circulation models. Mon. Weather Rev. 120 (6), 978–1002.
Morey, S., M. Koch, Y. Liu, and S. -K. Lee, 2017: Florida's oceans and marine habitats in a changing climate. In E. P. Chassignet, J. W. Jones, V. Misra, and J. Obeysekera (Eds.), Florida's climate: Changes, Variations, & Impacts (pp 391–425). Gainesville, FL: Florida Climate Institute. doi:10.17125/fci2017.ch13.
Moss, R.H., Edmonds, J.A., Hibbard, K.A., Manning, M.R., Rose, S.K., Van Vuuren, D.P., Carter, T.R., Emori, S., Kainuma, M., Kram, T., Meehl, G.A., 2010. The next generation of scenarios for climate change research and assessment. Nature 463 (7282), 747.
Nurse, L.A., Sem, G., 2001. Small island states. In: JT, Houghton., Ding, Y., Griggs, D.J., Noguer, M., van der Linden, P.J., Xiaosu, D. (Eds.), Climate Change 2001—The Scientific Basis. Contribution of Working Group 1 to the Third Assessment Report of the Intergovernmental Panel on Climate Change (IPCC). Cambridge University Press, Cambridge, pp. 843–875.
Peters, G.P., Andrew, R.M., Boden, T., Canadell, J.G., Ciais, P., Le Quéré, C., Marland, G., Raupach, M.R., Wilson, C., 2013. The challenge to keep global warming below 2°C. Nat. Clim. Chang. 3 (1), 4.
Putrasahan, D.A., Kamenkovich, I., Le Henaff, M., Kirtman, B.P., 2017. Importance of ocean mesoscale variability for air-sea interactions in the Gulf of Mexico. Geophys. Res. Lett. https://doi.org/10.1002/2017GL072884.
Rappaport, E.N., Franklin, J., 2010. Tropical cyclone intensity change before U. S. Gulf coast landfall. Wea. and Forecasting 25, 1380–1396.
Reichle RH, Liu Q (2014) Observation-Corrected Precipitation Estimates in GEOS-5.
Rousset, C., Beal, L.M., 2010. Observations of the Florida and Yucatan currents from a Caribbean cruise ship. J. Phys. Oceanogr. 40 (7), 1575–1581.
Sasaki, H., Klein, P., Qiu, B., Sasai, Y., 2014. Impact of oceanic-scale interactions on the seasonal modulation of ocean dynamics by the atmosphere. Nature Comm. https://doi.org/10.1038/ncomms6636.
Shchepetkin, A.F., McWilliams, J.C., 2005. The regional oceanic modeling system (ROMS): a split-explicit, free-surface, topography-following-coordinate oceanic model. Ocean Model. 9 (4), 347–404.
Sheinbaum, J., Candela, J., Badan, A., Ochoa, J., 2002. Flow structure and transport through the Yucatan Channel. Geophys. Res. Lett. 29 (3), 1040. https://doi.org/10.1029/2001GL013990.
Somot, S., Sevault, F., Déqué, M., 2006. Transient climate change scenario simulation of the Mediterranean Sea for the twenty-first century using a high-resolution ocean circulation model. Clim. Dyn. 27 (7–8), 851–879.
Somot, S., Sevault, F., Déqué, M., Crépon, M., 2008. 21st century climate change scenario for the Mediterranean using a coupled atmosphere–ocean regional climate model. Glob. Planet. Chang. 63, 112–126.
Stouffer, R.J., Yin, J., Gregory, J.M., Dixon, K.W., Spelman, M.J., Hurlin, W., Weaver, A.J., Eby, M., Flato, G.M., Hasumi, H., Hu, A., Jungclaus, J.H., Kamenkovich, I.V., Levermann, A., Montoya, M., Murakami, S., Nawrath, S., Oka, A., Peltier, W.R., Robitaille, D.Y., Sokolov, A., Vettoretti, G., Weber, S.L., 2006. Investigating the causes of the response of the Thermohaline Circulation to Past and Future climate. J. Climate 19, 1365–1387.
Suarez, M., Bacmeister, J., 2015. Development of the GEOS-5 atmospheric general circulation model: evolution from MERRA to MERRA2. Geosci. Model Dev. 8, 1339–1356. https://doi.org/10.5194/gmd-8-1339-2015.
Tan, I., Storelvmo, T., Zelinka, M.D., 2016. Observational constraints on mixed-phase clouds imply higher climate sensitivity. Science. 352 (6282), 224–227.
Tiedtke M (1983) The sensitivity of the time-mean large-scale flow to cumulus convection in the ECMWF model. In: Proceedings of ECMWF Workshop on Convective in Large-scale Models. European Centre for Medium-Range Weather Forecasts, Reading, United Kingdom. 297–316.
Umlauf, L., Burchard, H., 2003. A generic length-scale equation for geophysical turbulence models. J. Mar. Res. 61 (2), 235–265.
Vellinga, M., Wood, R.A., 2002. Impacts of thermohaline circulation shutdown in the twenty-first century. Clim. Chang. 54, 251–267.
Walsh, J., Wuebbles, D., Hayhoe, K., Kossin, J., Kunkel, K., Stephens, G., Thorne, P., Vose, R., Wehner, M., Willis, J., Anderson, D., Doney, S., Feely, R., Hennon, P., Kharin, V., Knutson, T., Landerer, F., Lenton, T., Kennedy, J., Somerville, R., 2014. Ch. 2: Our Changing Climate. Climate Change Impacts in the United States: The Third National

Climate Assessment, J. M. Melillo, Terese (T.C.) Richmond, and G. W. Yohe, Eds., U.S. Global Change. Research Program 19–67. https://doi.org/10.7930/J0KW5CXT.
Wargan, K., Coy, L., 2016. Strengthening of the tropopause inversion layer during the 2009 sudden stratospheric warming: a MERRA-2 study. J. Atmos. Sci. 73 (5), 1871–1887.
Wilby, R.L., Wigley, T.M., 1997. Downscaling general circulation model output: a review of methods and limitations. Prog. Phys. Geogr. 21 (4), 530–548.
Xu, Y., Fu, L., 2011. Global variability of the wavenumber spectrum of oceanic mesoscale turbulence. J. Phys. Oceanogr. 4, 802–809.
Yi, J., Schlesinger, M.E., Stouffer, R.J., 2009. Model projections of rapid sea-level rise on the northeast coast of the United States. Nat. Geosci. 2, 262–266.
Yin, J., Goddard, P.B., 2013. Oceanic control of sea level rise patterns along the east coast of the United States. Geophys. Res. Lett. https://doi.org/10.1002/2013GL057992.
Zhao, Q., Carr, F.H., 1997. A prognostic cloud scheme for operational NWP models. Mon. Weather Rev. 125 (8), 1931–1953.
Zhong, Y., Bracco, A., 2013. Submesoscale impacts on horizontal and vertical transport in the Gulf of Mexico. J. Geophys. Res. 104, 5651–5668.